IET Electric Power Applications

Research Article

IET Journals
The Institution of Engineering and Technology

Extended Kalman filter based estimations for improving speed-sensored control performance of induction motors

ISSN 1751-8660
Received on 22nd April 2020
Revised 26th June 2020
Accepted on 11th September 2020
E-First on 15th October 2020
doi: 10.1049/iet-epa.2020.0319
www.ietdl.org

Recep Yildiz[1], Murat Barut[1] ✉, Ridvan Demir[2]

[1]*Department of Electrical and Electronics Engineering, Niğde Ömer Halisdemir University, Niğde 51240, Turkey*
[2]*Department of Mechatronics Engineering, Niğde Ömer Halisdemir University, Niğde 51240, Turkey*
✉ *E-mail: mbarut@ohu.edu.tr*

Abstract: In this study, an extended Kalman filter (EKF)-based estimation algorithm is presented to improve the speed-sensored control performance of induction motors (IMs). The proposed EKF-based estimation algorithm is to simultaneously estimate the stator stationary axis components of stator currents and rotor fluxes, rotor angular speed, load torque including viscous friction term, rotor resistance and magnetising inductance in a single EKF algorithm without requiring any switching operation or a hybrid structure. In order to improve the speed-sensored control performance, the measurement/output matrix of IM model is extended by the measured rotor speed in addition to stationary axis components of the measured stator currents. Therefore, the proposed EKF algorithm uses the speed and stator current errors between the measured and priori estimation values in order to calculate the posterior estimation ones. For performance evaluation, the eighth order (proposed) EKF algorithm is tested by simulations and real-time experiments under challenging scenarios and compared with the developed sixth order EKF in real time. The obtained real-time results also show that the eighth order (proposed) EKF algorithm provides additional and improved estimations with the increased but feasible execution time in terms of the sixth order EKF designed in this paper.

1 Introduction

Although the high performance control of the induction motors (IMs) has been studied for a long time, it is still challenging area for the researchers. This challenge is due to varying both mechanical and electrical parameters in the highly non-linear model of IM. As it is well-known [1, 2], when IM starts running the following changes happen:

- The rotor resistance (R_r) and stator resistance (R_s) change according to the temperature and frequency (skin-effect).
- The magnetising inductance (L_m) depending on the flux level in the IM changes in the fleld-weakening region.
- Mechanical uncertainties occur due to variations in load torque (t_L) including friction.
- The additional difficulty is particularly faced at very low speeds due to increasing noise-signal ratio together with acquisition errors (measurement errors).

For obtaining the accurate and reliable calculations of the flux magnitude and flux angle utilised in any vector-based control of IMs, these varying parameters or uncertainties (especially R_s, R_r, L_m and t_L) together with measurement errors in the IM model need to be correctly known or estimated. Thus, different estimation methods are proposed [3–8] in order to overcome these uncertainties associated with the IM model. Considering the past speed-sensored studies [9–15] in the literature, rotor time constant estimation is performed by minimum order linear recursive least square algorithm in [9]. Shinohara *et al*. [10] presented an instantaneous active and reactive power based estimator to simultaneously estimate R_r and R_s together with a rotor flux observer to obtain the rotor flux angle and magnitude. However, authors emphasise that the convergence of the estimations is sensitive to load torque, and they conclude that the larger load leads to better convergence. Karanayil *et al*. [11] utilised a fuzzy logic and neural network estimators including a programmable cascade filter-based flux estimator for the on-line estimations of R_r and R_s, which requires time consuming design stages and computational load. Salmasi and Najafabadi [12] introduced an adaptive observer using single-phase current sensor in order to carry out the online estimations of stationary axis component of stator currents ($i_{s\alpha}$), stationary axis component of rotor fluxes ($\varphi_{r\alpha}$ and $\varphi_{r\beta}$) as well as the R_r and R_s. The designed observer is tested in both simulation and real-time experiments; however, its estimation performance is sensitive to variations in L_m and stator leakage inductance L_{ls}, and the presented results show that the larger inductance mismatch leads to more estimation error. Mapelli *et al*. [13] presented model reference adaptive systems (MRASs) utilising different methods known as reactive power and torque method for R_r estimation, and gives details about the sensitivity of the methods for different speed and load conditions. Yang *et al*. [14] proposed a MRAS-based estimator utilising the rotor fluxes, which are obtained by two sliding mode observers, for the estimations of R_r and L_m tested in both simulation and real-time experiments. Nevertheless, authors declare that even if the estimations of R_r and L_m are dependent on each other, the actual values of these parameters still can be estimated by time and for a better performance, it needs a decoupling method, which is designed in [15].

Along with other studies associated with the parameter estimations, one of the most widely used methods for the state and parameter estimation of IM is extended Kalman filter (EKF), which is an adaptation of Kalman filter for nonlinear systems. Differently from the other methods, the stochastic nature of EKFs is well suited to the uncertainties associated with the IM model [2]. Moreover, EKFs have ability to perform online estimations of states together with varying parameters under constant or changing rotor speed and torque in a relatively short time by taking system/process noise (modelling errors) and measurement noises/errors into account. From these points of view, EKFs are better but require more computational load than the other deterministic based methods [2]. However, developments in the processor technology remove this major drawback of EKFs and can be easily implemented with the acceptable execution times for real-time applications. Considering the EKF-based speed-sensored studies in the literature, [16] introduces an EKF algorithm performing on-line

© The Institution of Engineering and Technology 2020

estimations of $i_{s\alpha}$, $i_{s\beta}$, $\varphi_{r\alpha}$, $\varphi_{r\beta}$, R_r and R_s for direct vector control (DVC) of IM. The proposed EKF tested by both simulations and real-time experiments is sensitive to the variations in t_L. Demir *et al*. [17] executed the on-line estimation of $i_{s\alpha}$, $i_{s\beta}$, $\varphi_{s\alpha}$, $\varphi_{s\beta}$, R_r and R_s in simulation with utilisation of the stator flux-based IM model for the direct torque control (DTC) of IM while [18] simultaneously estimates $\varphi_{r\alpha}$, $\varphi_{r\beta}$, R_r and L_m in both simulation and real-time experiments by utilising a reduced-order EKF including rotor flux based IM model. However, the estimation performances of the proposed methods by [17, 18] require the accurate t_L. There are also the EKF-based speed-sensorless studies as in [2, 19–23] for the states and parameters estimations of IMs. Yildiz *et al*. [19] presented a comprehensive comparison of extended and unscented Kalman filter algorithms for speed-sensorless control applications of IMs by investigating the effect of noise covariance matrices, parameter changes, sampling time and computational burdens on estimation performance of both algorithms. In [20], speed and flux are estimated by a multiple model EKF including single models with different process covariance matrices ($\boldsymbol{Q}$) in order to take the range of $\boldsymbol{Q}$ in consideration. In order to increase the number of estimated states and parameters of IM, the switching and braided EKF ([2, 21]) utilising consecutively two EKF algorithms with different IM models and bi input EKF ([22, 23]) including a single EKF algorithm using consecutively two inputs based on two different seventh order IM models. Although the bi input EKF reduces the required memory area for embedding algorithm and provides easier debugging and design in terms of the switching and braided EKFs, it still demands more computational load, more memory and the design complexity considering a standard EKF algorithm utilising a single IM model. Moreover, the bi input EKF technique using two different models requires the higher number elements of noise covariance matrices to be tuned due to two different IM models, which makes the tuning process difficult and challenging.

The main contribution of this study is to introduce an EKF algorithm with the help of a single eighth order IM model including the extended measured states for the on-line estimations of $i_{s\alpha}$, $i_{s\beta}$, $\varphi_{r\alpha}$, $\varphi_{r\beta}$, ω_m, t_L, R_r and L_m. Differently from the past EKF-based speed-sensored studies including the performance deteriorations due to the variations in t_L as in [16–18], ω_m is defined as a state in the IM model with the utilisation of the equation of motion, which allows:

- To estimate t_L in this paper.
- To take the rotor speed errors together with the stator current errors into account in calculating or correcting the estimations of the unmeasured states in the proposed EKF algorithm.

Finally, the eighth order (proposed) EKF algorithm is tested by simulations and real-time experiments under challenging variations in ω_m, t_L, R_r and L_m as well as changes in leakage inductances and compared with the sixth order EKF with the estimations of $i_{s\alpha}$, $i_{s\beta}$, $\varphi_{r\alpha}$, $\varphi_{r\beta}$, R_r and L_m by measuring $i_{s\alpha}$, $i_{s\beta}$ and ω_m in real-time. The obtained results confirm the effectiveness of the proposed EKF algorithm and illustrate that the eighth order (proposed) EKF algorithm gives the additional and improved estimations with the increased but acceptable execution time in terms of the sixth order EKF designed in this paper.

This paper is organised as follows: Section 1 presents the literature review of past studies related to state and parameters estimation of IMs. In Section 2, the eighth order extended IM model is given. Section 3 introduces the development of the proposed EKF algorithm. Simulation results and observations are presented in Section 4. The experimental setup and real-time experimental results are given in Sections 5 and 6, respectively. Finally, Section 7 provides the conclusion.

2 Development of extended induction motor model

In this study, the eighth order IM model is introduced to obtain more robust state and parameter estimation performance with the utilisation of the proposed EKF algorithm by increasing the number of estimated parameters whose values change with the working conditions of IM. For this purpose, the rotor flux based IM model developed for the simultaneous estimation of $i_{s\alpha}$, $i_{s\beta}$, $\varphi_{r\alpha}$, $\varphi_{r\beta}$, ω_m, t_L, R_r and L_m is given in (1) and (2) with the general form. In the eighth order IM model, t_L, R_r and L_m are determined as constant states by assuming that their values change slowly with respect to the time and working conditions [23]

$$\begin{aligned} \boldsymbol{x}_{k+1} &= \boldsymbol{f}(\boldsymbol{x}_k, \boldsymbol{u}_k) + \boldsymbol{w}_k \\ &= \boldsymbol{A}(\boldsymbol{x}_k)\boldsymbol{x}_k + \boldsymbol{B}\boldsymbol{u}_k + \boldsymbol{w}_k \end{aligned} \tag{1}$$

$$\begin{aligned} \boldsymbol{z}_k &= \boldsymbol{h}(\boldsymbol{x}_k) + \boldsymbol{v}_k \\ &= \boldsymbol{H}\boldsymbol{x}_k + \boldsymbol{v}_k \end{aligned} \tag{2}$$

Here $\boldsymbol{x}$ is extended state vector, $\boldsymbol{u}$ is control input vector, $\boldsymbol{w}$ is process noise, $\boldsymbol{v}$ is measurement noise, $\boldsymbol{f}$ is the non-linear state and input function, $\boldsymbol{h}$ is the output function, $\boldsymbol{A}$ is the extended system matrix, $\boldsymbol{B}$ is control input matrix, $\boldsymbol{H}$ is the measurement matrix and $\boldsymbol{z}$ is the measurement vector. In the same manner with the presented general form in (1) and (2), the detailed matrix representation of the IM model is given in (3) and (4) as below:

(see (3))

$$\underbrace{\begin{bmatrix} i_{s\alpha,k} \\ i_{s\beta,k} \\ \omega_{m,k} \end{bmatrix}}_{\boldsymbol{z}_k} = \underbrace{\begin{bmatrix} 1 & 0 & 0 & 0 & 0 & 0 & 0 & 0 \\ 0 & 1 & 0 & 0 & 0 & 0 & 0 & 0 \\ 0 & 0 & 0 & 0 & 1 & 0 & 0 & 0 \end{bmatrix}}_{\boldsymbol{H}} \underbrace{\begin{bmatrix} i_{s\alpha,k} \\ i_{s\beta,k} \\ \varphi_{r\alpha,k} \\ \varphi_{r\beta,k} \\ \omega_{m,k} \\ t_{L,k} \\ R_{r,k} \\ L_{m,k} \end{bmatrix}}_{\boldsymbol{x}_k} + \boldsymbol{v}_k \tag{4}$$

$$a_1 = \left(R_s + \frac{R_{r,k}L_{m,k}^2}{L_{r,k}^2}\right)\frac{T}{L_{\sigma,k}},\ a_2 = \frac{R_{r,k}L_{m,k}}{L_{r,k}^2 L_{\sigma,k}}T,$$

$$\underbrace{\begin{bmatrix} i_{s\alpha,k+1} \\ i_{s\beta,k+1} \\ \varphi_{r\alpha,k+1} \\ \varphi_{r\beta,k+1} \\ \omega_{m,k+1} \\ t_{L,k+1} \\ R_{r,k+1} \\ L_{m,k+1} \end{bmatrix}}_{\boldsymbol{x}_{k+1}} = \underbrace{\begin{bmatrix} 1-a_1 & 0 & a_2 & a_3 & 0 & 0 & 0 & 0 \\ 0 & 1-a_1 & -a_3 & a_2 & 0 & 0 & 0 & 0 \\ a_4 & 0 & 1-a_5 & -a_6 & 0 & 0 & 0 & 0 \\ 0 & a_4 & a_6 & 1-a_5 & 0 & 0 & 0 & 0 \\ -a_7 & a_8 & 0 & 0 & 1 & -a_9 & 0 & 0 \\ 0 & 0 & 0 & 0 & 0 & 1 & 0 & 0 \\ 0 & 0 & 0 & 0 & 0 & 0 & 1 & 0 \\ 0 & 0 & 0 & 0 & 0 & 0 & 0 & 1 \end{bmatrix}}_{\boldsymbol{A}(\boldsymbol{x}_k)} \underbrace{\begin{bmatrix} i_{s\alpha,k} \\ i_{s\beta,k} \\ \varphi_{r\alpha,k} \\ \varphi_{r\beta,k} \\ \omega_{m,k} \\ t_{L,k} \\ R_{r,k} \\ L_{m,k} \end{bmatrix}}_{\boldsymbol{x}_k} + \underbrace{\begin{bmatrix} b_1 & 0 \\ 0 & b_1 \\ 0 & 0 \\ 0 & 0 \\ 0 & 0 \\ 0 & 0 \\ 0 & 0 \\ 0 & 0 \end{bmatrix}}_{\boldsymbol{B}} \underbrace{\begin{bmatrix} u_{s\alpha,k} \\ u_{s\beta,k} \end{bmatrix}}_{\boldsymbol{u}_k} + \boldsymbol{w}_k \tag{3}$$

© The Institution of Engineering and Technology 2020

$$a_3 = \frac{L_{\mathrm{m},k}\omega_{\mathrm{m},k}}{L_{\sigma,k}L_{\mathrm{r},k}}p_{\mathrm{p}}T,\ a_4 = \frac{R_{\mathrm{r},k}}{L_{\mathrm{r},k}}L_{\mathrm{m},k}T,$$

$$a_5 = \frac{R_{\mathrm{r},k}}{L_{\mathrm{r},k}}T,\ a_6 = p_p\omega_{\mathrm{m},k}T,\ a_7 = \frac{3}{2}\frac{p_{\mathrm{p}}}{J_t}\frac{L_{\mathrm{m},k}}{L_{\mathrm{r},k}}\varphi_{\mathrm{r}\beta,k}T,$$

$$a_8 = \frac{3}{2}\frac{p_{\mathrm{p}}}{J_t}\frac{L_{\mathrm{m},k}}{L_{\mathrm{r},k}}\varphi_{\mathrm{r}\alpha,k}T,\ a_9 = \frac{T}{J_t},\ b_1 = \frac{T}{L_{\sigma,k}},$$

$$L_{s,k} = L_{ls} + L_{m,k},\ L_{r,k} = L_{lr} + L_{m,k}$$

where L_{s}, L_{ls}, L_{r} and L_{lr} are the stator inductance and its leakage inductance as well as rotor inductance and its leakage inductance, respectively; R_{s} and $L_\sigma = \sigma L_{\mathrm{s}}$ stator resistance and transient inductance, respectively; $\sigma = 1 - L_{\mathrm{m}}^2/(L_{\mathrm{r}}L_{\mathrm{s}})$ is the leakage factor; J_t is the summation of IM and load inertia; p_{p} is the number of pole pairs; $u_{\mathrm{s}\alpha}$ and $u_{\mathrm{s}\beta}$ are the stationary axis components of stator voltages and T is the sampling time.

3 Proposed EKF algorithm

Contrary to the other EKF-based speed-sensored IM control studies [16–18], the measurement matrix given in (4) is extended by the measured mechanical speed information in order to take speed measurement errors into account for correcting estimations. Namely, the speed error which is determined by the difference between the measured and estimated speeds is also used for the posterior estimation value of states and parameters along with the $i_{s\alpha}$ and $i_{s\beta}$ error information in EKF. This extension helps to increase the number of estimated states and parameters without using any switching operation as in [22, 23]. For this purpose, the conventional EKF equations used for the simultaneous estimation of the states and parameters given in (3) and (4) are presented below in detail.

(i) Determination of initial conditions:

$$\hat{\boldsymbol{x}}_0 = E[\boldsymbol{x}_0] \tag{5}$$

$$\boldsymbol{P}_0 = E\left[(\boldsymbol{x}_0 - \hat{\boldsymbol{x}}_0)(\boldsymbol{x}_0 - \hat{\boldsymbol{x}}_0)^{\mathrm{T}}\right] \tag{6}$$

(ii) Linearisation step:

$$\boldsymbol{F}_{k+1|k} = \left.\frac{\partial \boldsymbol{f}_{\mathrm{e}}(\boldsymbol{x}, \boldsymbol{u}_k)}{\partial \boldsymbol{x}}\right|_{\boldsymbol{x}=\boldsymbol{x}_k} \tag{7}$$

(iii) Estimation or time update steps:

$$\hat{\boldsymbol{x}}_k^- = \boldsymbol{f}_{\mathrm{e}}(\hat{\boldsymbol{x}}_{k-1}, \boldsymbol{u}_k) \tag{8}$$

$$\boldsymbol{P}_k^- = \boldsymbol{F}_{k|k-1}\boldsymbol{P}_{k-1}\boldsymbol{F}_{k|k-1}^{\mathrm{T}} + \boldsymbol{Q}_{k-1} \tag{9}$$

(iv) Correction or measurement update steps:

$$\boldsymbol{K}_k = \boldsymbol{P}_k^-\boldsymbol{H}^{\mathrm{T}}\left[\boldsymbol{H}\boldsymbol{P}_k^-\boldsymbol{H}^{\mathrm{T}} + \boldsymbol{R}_k\right]^{-1} \tag{10}$$

$$\hat{\boldsymbol{x}}_k = \hat{\boldsymbol{x}}_k^- + \boldsymbol{K}_k(\boldsymbol{z}_k - \boldsymbol{H}\hat{\boldsymbol{x}}_k^-) \tag{11}$$

$$\boldsymbol{P}_k = (\boldsymbol{I} - \boldsymbol{K}_k\boldsymbol{H})\boldsymbol{P}_k^- \tag{12}$$

Here, $\boldsymbol{F}$ represents the linearised non-linear model; $\hat{\boldsymbol{x}}^-$ and $\hat{\boldsymbol{x}}$ represent the priori and the posteriori state and parameter estimations, respectively; $\boldsymbol{P}^-$ and $\boldsymbol{P}$ represent the priori and the posteriori error covariance; $\boldsymbol{Q}$ and $\boldsymbol{R}$ represent the process and measurement covariance matrices, respectively; $\boldsymbol{K}$ and $\boldsymbol{I}$ represent the Kalman gain and Identity matrix, respectively.

4 Simulation results

In this part, the proposed EKF-based estimation algorithm with the help of the extension of the $\boldsymbol{H}$ matrix is tested under challenging scenarios in the simulation using Matlab Simulink. Besides, the EKF-based speed-sensored IM drive, capable to carry out the field-weakening operation, which is involved in magnitude and phase angle ($\hat{\theta}_{\mathrm{rf}}$) of the rotor flux information to perform the control is given in Fig. 1. Even though the estimations of t_{L} and R_{r} parameters are not required for the control algorithm as shown in Fig. 1, those values are estimated to increase the estimation performance of the states utilised in the control algorithm under the different working conditions that result in the parameter changes. In addition, estimated L_{m} is utilised to increase robustness of the control system in field-weakening region. Furthermore, Table 1 contains the rated IM parameter values that are the same as the past studies [18, 23] in order to make a fair comparison at the same motor parameters.

In order to demonstrate the effectiveness of the proposed EKF-based IM drive, it is tested under challenging scenarios that particularly occur to force the estimator. Reference signals applied to the proposed IM drive for the challenging scenarios are presented in Fig. 2 as well as the estimation results and errors of EKF are given in Figs. 3 and 4, respectively. Here, $n_{\mathrm{m}}^{\mathrm{ref}}$ is the speed reference, $|\vec{\boldsymbol{\varphi}}_{\mathrm{r}}|^{\mathrm{ref}}$ is the flux magnitude reference, '$\hat{\cdot}$' represents the estimated values and '$e_{(.)}$' represents the difference between actual and estimated value apart from $e_{|\boldsymbol{\varphi}_{\mathrm{r}}|}$, which refers to the difference between the reference and estimated rotor flux magnitude. On the other hand, once the motor operates in the field-weakening region which is performed by increasing speed reference, in contrast to magnitude of the flux reference, the magnetising inductance

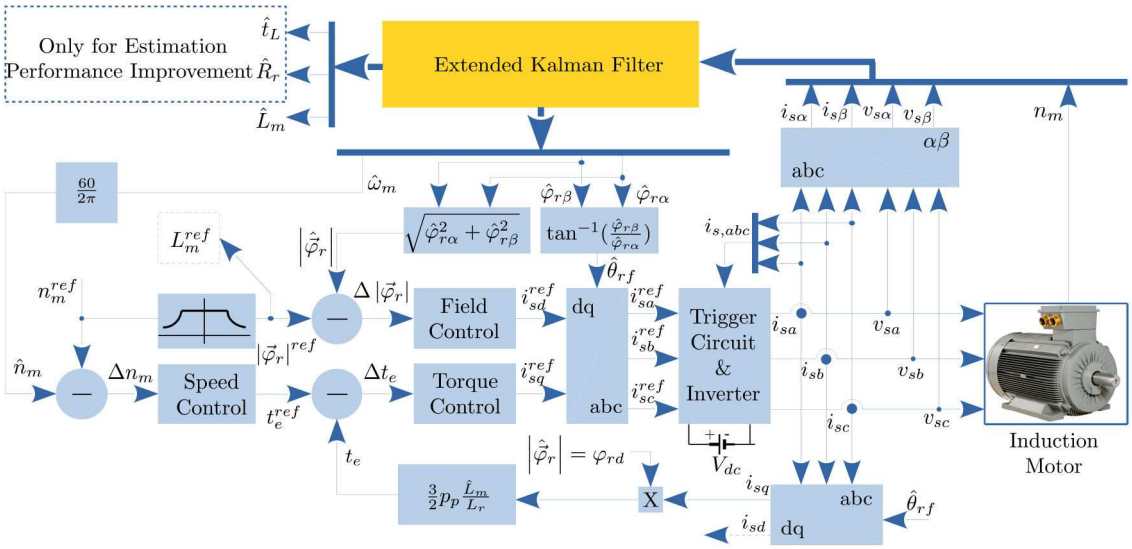


Fig. 1 *EKF-based speed-sensored IM drive used in simulations*

© The Institution of Engineering and Technology 2020

Table 1 Rated values and parameters of the IM used in simulations

P, kW	V, V	I, A	f, Hz	N_m, rpm	t_L, N . m	p_p	R_s, Ω	R_r, Ω	L_s, H	L_r, H	L_m, H	J_t, kg . m^2	B_t, Nm/(rad/s)
2	380	6.9	50	1430	20	2	2.283	2.133	0.2311	0.2311	0.22	0.0183	0.001

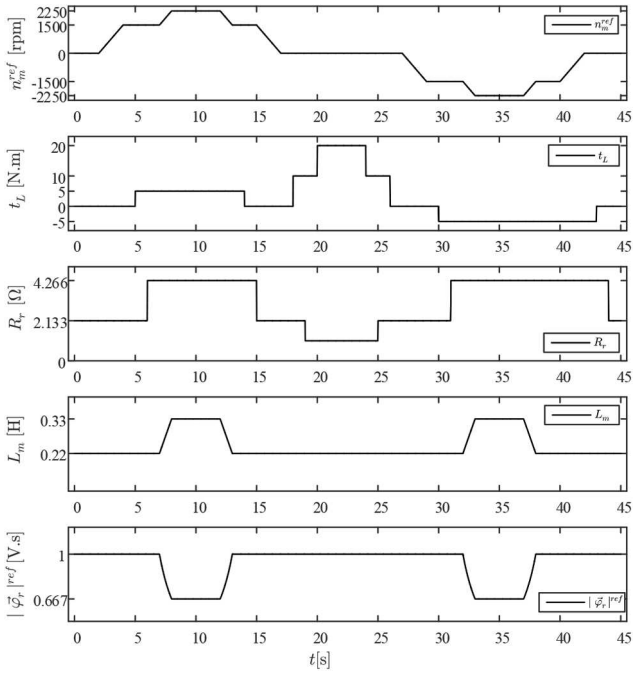


Fig. 2 *Reference signals of simulation tests*

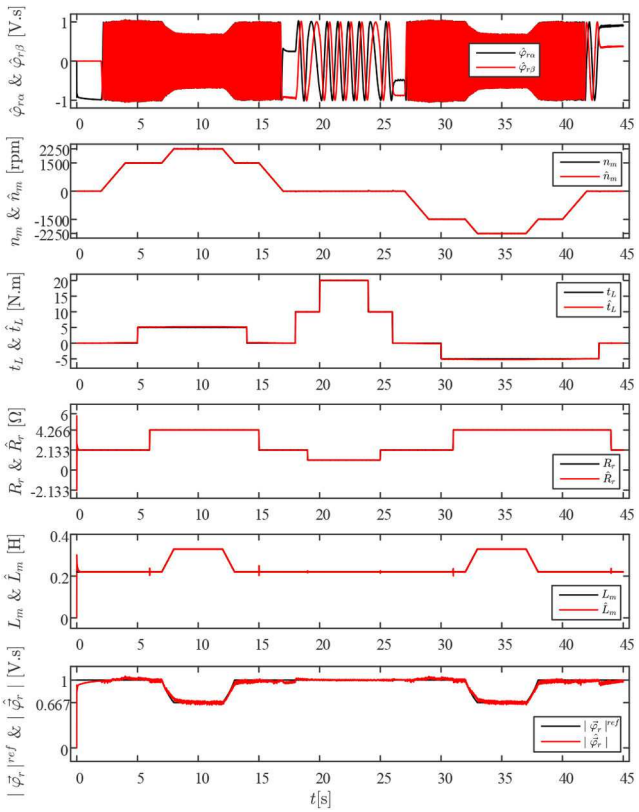


Fig. 3 *Simulation results of EKF-based estimation and control*

reference value increases as shown in Fig. 2. This situation occurs due to the DC voltage limit of the inverter given in Fig. 1 [23–25]. How magnetising inductance reference changes is given in (13) and (14). Here, $|\boldsymbol{\varphi}_r|_{rated}$ is rated flux reference. n_{mb} and L_{mb} are the base speed (equaling to its rated value, 1500 rpm) and base magnetising inductance (equaling to rated magnetising inductance value, 0.22 H) of the IM, respectively.

- For $n_m^{ref} > n_{mb}$

$$\left|\boldsymbol{\varphi}_r\right|^{ref} = \frac{n_{mb}}{n_m^{ref}}\left|\boldsymbol{\varphi}_r\right|_{rated}, \; L_m^{ref} = \frac{|\boldsymbol{\varphi}_r|_{rated}}{|\boldsymbol{\varphi}_r|^{ref}}L_{mb} \tag{13}$$

- For $n_m^{ref} \leqslant n_{mb}$

$$\left|\boldsymbol{\varphi}_r\right|^{ref} = 1, \; L_m^{ref} = L_{mb} \tag{14}$$

For the simulation studies, the noise covariance matrices ($\boldsymbol{Q}$ and $\boldsymbol{R}$) that affect the estimation performance of EKF are chosen by trial-and-error method. Furthermore, $\boldsymbol{Q}$ and $\boldsymbol{R}$ are chosen as constant and diagonal form in order to both reduce the computational burden and guarantee the positive definiteness. The chosen values for these matrices are $\boldsymbol{Q} = \text{diag}\{10^{-6}, 10^{-6}, 10^{-12}, 10^{-12}, 10^{-3}, 10^{-3}, 5\times10^{-6}, 3\times10^{-7}\}$, $\boldsymbol{R} = \text{diag}\{10^{-7}, 10^{-7}, 10^{-3}\}$ and $\boldsymbol{P}_0 = \text{diag}\{10, 10, 10, 10, 10, 10, 10, 10\}$. Besides, the sample time for the simulation studies is determined as $T = 100\,\mu$s.

Considering the estimation results of EKF with the help of the extended $\boldsymbol{H}$ matrix and thus the control performance of the proposed EKF-based IM drive, the following remarks for Figs. 3 and 4 can be made:

- Although all initial conditions of the estimated states and parameters are chosen as zero, those values converge to their actual ones as soon as possible.
- However, the scenario contains the step-like changes of t_L and R_r for both high-speed and zero speed operations of IM. It is observed that the proposed EKF shows a very satisfying performance under these challenging conditions and quickly generates the correct estimation results, as can be seen from the presented estimation errors in Fig. 4.
- For the field-weakening region that refers to L_m variation, even if IM operates under 5 N m load with two times bigger R_r value than its rated, the proposed EKF algorithm easily handles the challenging condition that is specially designed to force EKF.
- In some cases, the worst scenario called DC condition is performed more than once to test the robustness of estimator. Nevertheless, it can be seen in the results that both proposed algorithm and thus IM drive are quite good to overcome this challenge.
- Finally, there is a bias in Fig. 4 at e_{t_L} for steady-state operation, which is not a real estimation error. The reason for the bias is that the IM model given in (3) and (4) does not include the viscous friction term, thus, this bias represents this term as mathematically proved below:

$$e_{t_L} \cong -\beta_L \omega_m(\infty)$$

  - For $n_m = 1500$ rpm

$$0.157 \cong -0.001 \times \frac{-1501 \times 2 \times \pi}{60}$$

$$0.157 \cong 0.15718$$

  - For $n_m = 2250$ rpm

$$0.235 \cong -0.001 \times \frac{-2250 \times 2 \times \pi}{60}$$

$$0.235 \cong 0.23561$$

© The Institution of Engineering and Technology 2020

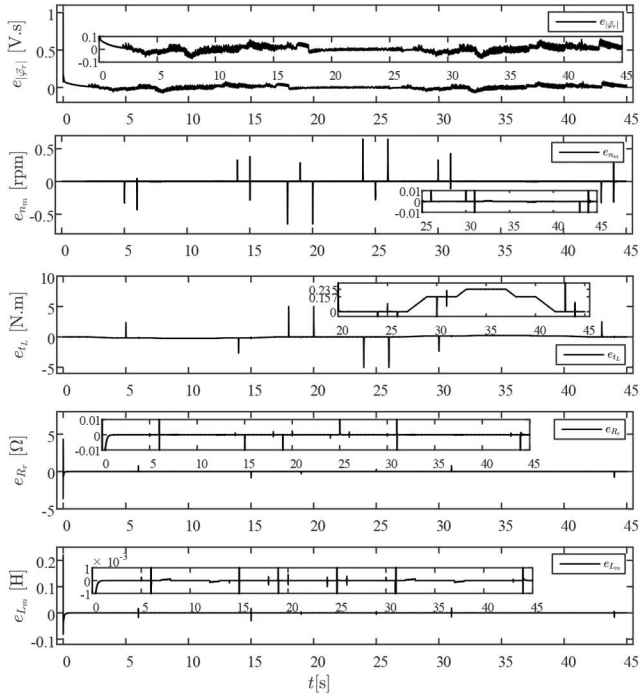


Fig. 4 *Simulation results of EKF-based estimation and tracking errors*

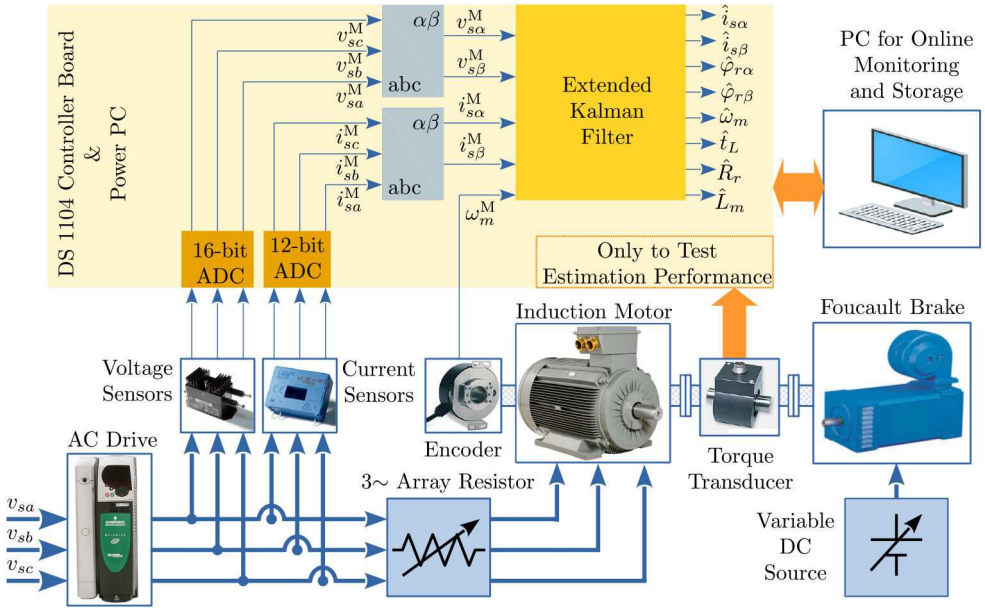


Fig. 5 *Experimental setup for performance tests*

Table 2 Rated values and Parameters of the IM Used in real time experiments

P, kW	V, V	I, A	f, Hz	N_m, rpm	t_L, N . m	p_p	R_s, Ω	R_r, Ω	L_s, H	L_r, H	L_m, H	J_t, kg . m^2	B_t, Nm/(rad/s)
2.2	380	5.5	50	950	20	3	3	2.53	0.0116	0.0174	0.135	0.055	0.001

5 Hardware configuration

In order to verify the effectiveness of the proposed EKF in real-time, the experimental setup illustrated in Fig. 5 is utilised. The rated specifications of three phase squirrel cage IM and the Foucault brake loading the IM up to 30 N.m are given in Table 2. The 50 N.m torque transducer is only utilised to verify the load torque estimation of the proposed EKF. The rotor mechanical speed, stator currents and stator voltages are measured by an encoder with 5000 lines/rev, LA55-P/SP1 and LV 100-400, respectively. The proposed EKF algorithm in Matlab S-function block derived in C/C++ language is implemented on DS1104 controller board with 250 MHz 64-bit floating-point processor. For a more realistic performance evaluation of the proposed EKF algorithm, the IM is supplied by the AC drive applying the pulse-width modulated voltages, as seen in Fig. 5.

6 Real-time experimental results

The effectiveness of the EKF algorithm is tested by using the experimental setup in Fig. 5 under different challenging scenarios including variations of ω_m, t_L, R_r, L_m, L_{ls} and L_{lr} in real-time experiments. In order to generate the step-like changes in R_r and L_m at a constant speed for these real-time scenarios, the method in [26] is utilised for this paper as below:

- First, R_r and L_m are defined as

© The Institution of Engineering and Technology 2020

$$R_{\mathrm{r}} = R_{\mathrm{rn}} \times \hat{\chi} \tag{15}$$

$$L_{\mathrm{m}} = L_{\mathrm{mn}} \times \hat{\Upsilon} \tag{16}$$

Here R_{rn} and L_{mn} are the rated R_{r} and L_{m} values given in Table 2. $\hat{\chi}$ and $\hat{\Upsilon}$ are the estimated uncertainties related to R_{r} and L_{m}, respectively.

- Second, $R_{\mathrm{rn}} \times \hat{\chi}$ and $L_{\mathrm{mn}} \times \hat{\Upsilon}$ are substituted for $\boldsymbol{A}$ and $\boldsymbol{B}$ in (3) instead of R_{r} and L_{m}, respectively.
- Finally, $\hat{\chi}$ and $\hat{\Upsilon}$ are included to $\boldsymbol{x}_{k+1}$ and $\boldsymbol{x}_k$ vectors in (3) and (4) as new states instead of R_{r} and L_{m}, respectively.

In this method, when the IM is operating under the rated conditions with the correct values of R_{rn} and L_{mn}, $\hat{\chi}$ and $\hat{\Upsilon}$ should converge to 1. However, if the correct values of R_{rn} and L_{mn} are unknown and taken as $R_{rn}/2$ and $2 \times L_{\mathrm{mn}}$ then $\hat{\chi}$ and $\hat{\Upsilon}$ reach to 2 and 0.5 at steady-state, respectively. That is why they are considered to represent uncertainties associated with R_{r} and L_{m}.

On the other hand, the initial conditions of the EKF-based estimation algorithm are taken as zero for all estimated states and parameters with the sampling time of $T = 100\,\mu\mathrm{s}$ and the noise covariance matrices are chosen by trial-and-error method as $\boldsymbol{Q} = \mathrm{diag}\{10^{-10}, 10^{-10}, 10^{-12}, 10^{-12}, 10^{-5}, 10^{-4}, 10^{-5}, 10^{-5}\}$, $\boldsymbol{R} = \mathrm{diag}\{10^{-4}, 10^{-4}, 10^{-4}\}$ and $\boldsymbol{P}_0 = \mathrm{diag}\{10, 10, 10, 10, 10, 10, 10, 10\}$.

In order to demonstrate the performance of the estimation algorithm with the extended $\boldsymbol{H}$ matrix, the different challenging scenarios and observations are considered as below.

6.1 Scenario 1: step-like changes in t_{L} at constant speed

This scenario aims to test the estimation performance of the proposed EKF algorithm against the step-like changes in t_{L} in a real-time experiment as shown in Figs. 6 and 7. The instant variations of t_{L} in Figs. 6 and 7 are generated by applying step-like voltages to the Foucault brake while the IM operates at the rated speed. From the obtained results in Figs. 6 and 7, it is clear that $\hat{t}_{\mathrm{L}}$ satisfactorily tracks t_{L} in spite of switching t_{L} from its rated value to zero or vice versa.

6.2 Scenario 2: step-like changes in R_{r} and L_{m} at constant speed and rated torque/no-load

In this scenario, the step-like uncertainties of $\hat{\chi}$ and $\hat{\Upsilon}$ related to R_{r} and L_{m} are tested at a constant (rated) speed and rated torque/no-load, as demonstrated in Figs. 8 and 9. In order to force the proposed EKF, the large instant uncertainties in R_{r} and L_{m} are generated by taking

- R_{rn} as $R_{\mathrm{rn}}/2$ at 5 s and R_{rn} at 15 s and L_{mn} as $L_{\mathrm{mn}}/2$ at 10 s and L_{mn} at 20 s at the rated torque
- R_{rn} as $2 \times R_{\mathrm{rn}}$ at 30 s and R_{rn} at 40 s and L_{mn} as $2 \times L_{\mathrm{mn}}$ at 35 s and L_{mn} at 45 s at no-load.

Moreover, the step-like variation on the rotor speed occurs due to unloading IM. However, those step-like uncertainties of $\hat{\chi}$ and $\hat{\Upsilon}$ at the rated torque/no-load are quickly estimated by the proposed EKF; thus, there is no estimation error on the other estimated states as inspecting Figs. 8 and 9.

6.3 Scenario 3: speed and torque reversal

This scenario presents the challenging performance test of the proposed EKF under linear variations of n_{m}, t_{L} and R_{r}, as given in Figs. 10 and 11. Although t_{L} and R_{r} are defined as constant states in (3), they are linearly changed at the same time together with n_{m} in clock wise and counter clock wise directions with zero speed transitions. Nevertheless, very acceptable results are obtained.

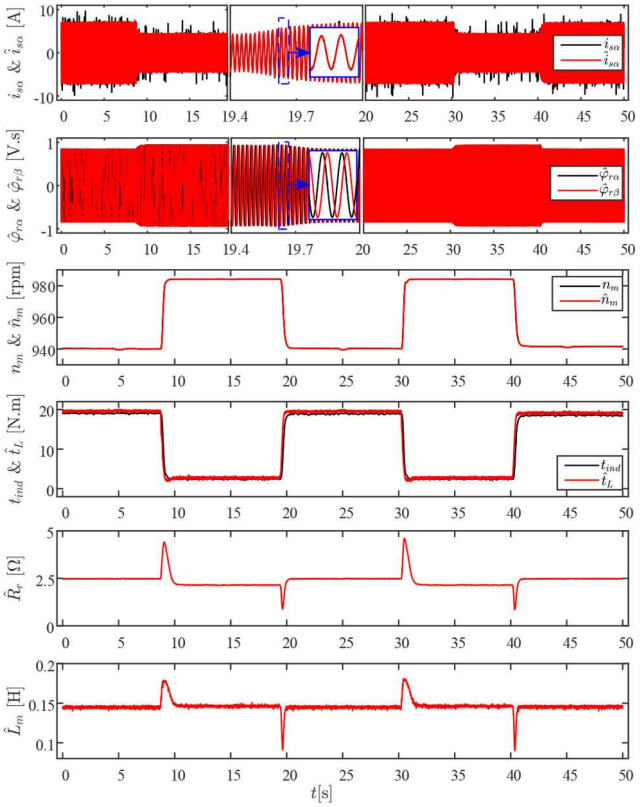


Fig. 6 *Real-time experimental results of proposed EKF for Scenario 1*

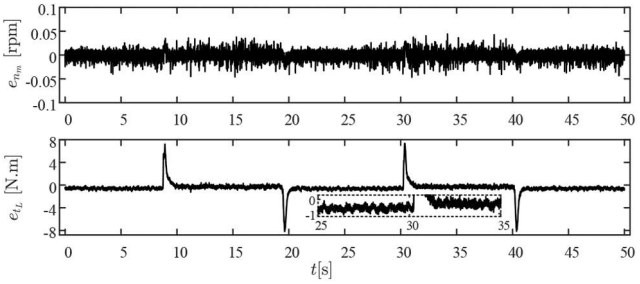


Fig. 7 *Real-time experimental results of EKF-based estimation error associated with n_m and t_L for Scenario 1*

Namely, all of estimated states and parameters immediately converge actual ones. According to [27], the variation in R_{r} changes with the rotor/slip frequency (f_{r}) (skin effect) and rotor temperature. Proca and Keyhani [27] also discovered the linear relationship (within the range of interest) between R_{r} and f_{r}. To investigate the influence of f_{r} on R_{r} in this study as in [22, 26], slip compensation is disabled in the ac drive and f_{r} is calculated by using (17) and shown in Fig. 10

$$f_{\mathrm{r}} = f_{\mathrm{s}} - p_{\mathrm{p}} \times \frac{n_{\mathrm{m}}}{60} \tag{17}$$

Here, f_{s} is the stator frequency. As seen from Fig. 10, the variations of $\hat{\chi}$ and f_{r} changing from 1.75 Hz in clockwise direction to 1.88 Hz in counter clockwise direction reveal the linear relationship between f_{r} and R_{r}, and they are also matched with the results demonstrated in [22, 26, 27].

6.4 Scenario 4: observations on estimation performance for the changes in leakage inductances

In an efficiently designed and manufactured IMs, the stator leakage inductance (L_{ls}) and rotor leakage inductance referred to the stator side (L_{lr}) are always small in terms of L_{m}; total leakage inductance ($L_\sigma = L_{\mathrm{lr}} + L_{\mathrm{ls}}$) and thus L_{ls} and L_{lr} can be easily determined by the

© The Institution of Engineering and Technology 2020

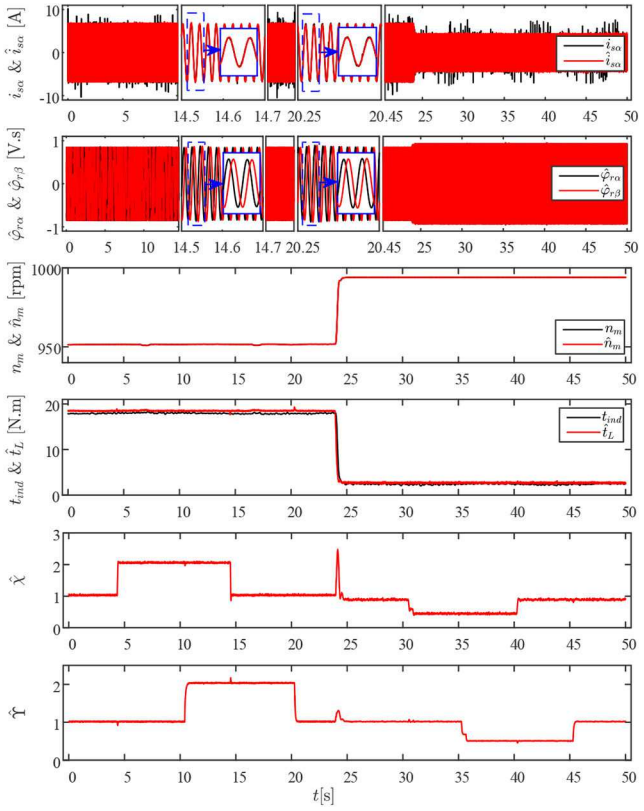


Fig. 8 *Real-time experimental results of proposed EKF for Scenario 2*

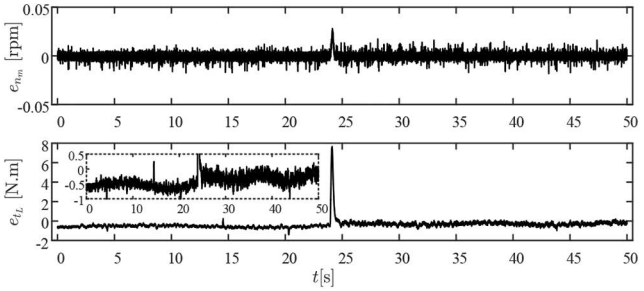


Fig. 9 *Real-time experimental results of EKF-based estimation error associated with n_m and t_L for Scenario 2*

IEEE Standard 112-1996 Test Procedure for Polyphase Induction Motors and Generators [28] or the other methods as in [29–31]. The load-dependent variations about 20% [32] in L_σ, L_{ls} or L_{lr} are usually ignored in the estimation and control performances since they are less important on the performances than R_r and L_m [31]. Thus, this paper considers the estimation of R_r and L_m together with t_L and also investigates the effects of incorrect values of L_{ls} or L_{lr} on the estimation performance of the proposed EKF algorithm, as seen in Figs. 12 and 13. Here, while the IM runs at rated speed and underrated load torque the following changes of ±50% are generated:

- First, L_{lr} and L_{ls} are stepped up to $1.5 \times L_{lrn}$ at 7 s and $1.5 \times L_{lsn}$ at 15 s, respectively.
- Next, L_{lr} and L_{ls} are returned to L_{lrn} at 22 s and L_{lsn} at 33 s, respectively.
- Later, L_{lr} and L_{ls} are stepped down to $0.5 \times L_{lrn}$ at 40 s and $0.5 \times L_{lsn}$ at 47 s, respectively.
- Finally, L_{lr} and L_{ls} are returned to L_{lrn} at 56 s and L_{lsn} at 65 s, respectively.

As seen from the obtained results in Figs. 12 and 13, these very large incorrect values of L_{ls} or L_{lr} (and thus L_σ) do not give rise to any estimation error in the estimated speed ($\hat{n}_m$) and load torque

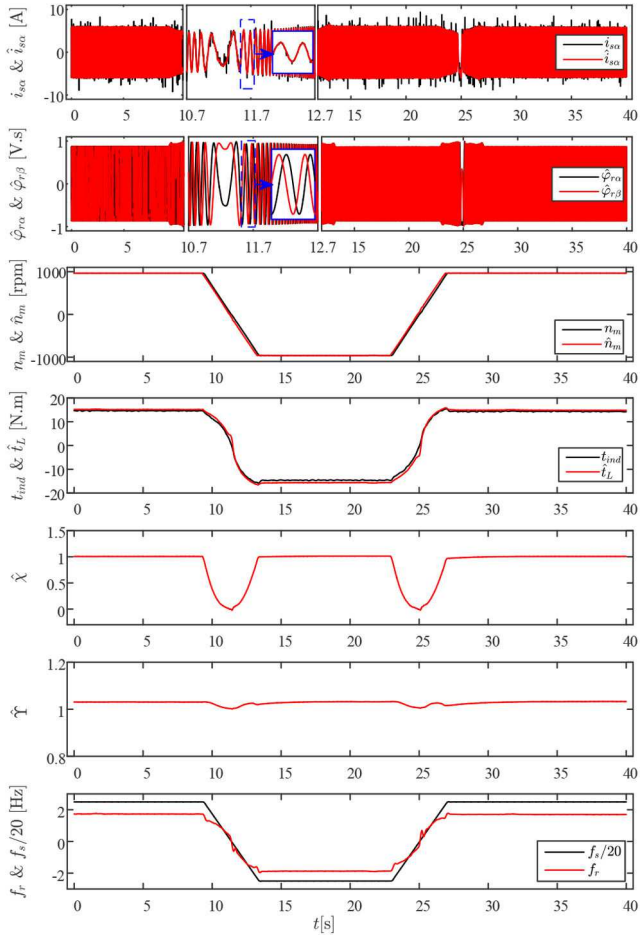


Fig. 10 *Real-time experimental results of proposed EKF for Scenario 3*

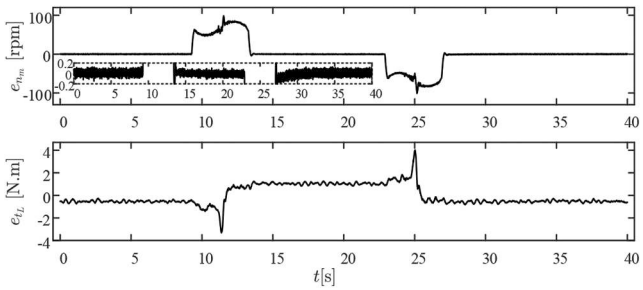


Fig. 11 *Real-time experimental results of EKF based estimation error associated with n_m and t_L for Scenario 3*

($\hat{t}_L$) together with the other estimated states and parameters since $\hat{\chi}$ and $\hat{\Upsilon}$ are able to compensate these incorrect values of L_{ls} or L_{lr} (and thus L_σ) by regulating their values. This reality is confirmed by operating the IM model with the incorrect values of L_{ls} or L_{lr} (and thus L_σ) in real-time, and then it is observed that the incorrect values cause errors in the states of the IM model including $\chi = \Upsilon = 1$, but when Υ is increased to 1.083 and χ is reduced to 0.976 at the same instant, they become equal to their correct values; Therefore, $\hat{\chi}$ and $\hat{\Upsilon}$ in Figs. 12 and 13 are indirectly verified that they (and thus the proposed EKF-based estimation algorithm in this paper) are able to correct the estimations under the uncertainties associated with L_{ls} or L_{lr} (and thus L_σ).

6.5 Observations on comparison of the eighth order (proposed) and the sixth order EKFs

In this section, it is aimed to compare the eighth order (proposed) EKF with the estimations of $i_{s\alpha}$, $i_{s\beta}$, $\varphi_{r\alpha}$, $\varphi_{r\beta}$, ω_m, t_L, R_r and L_m and sixth order EKF with the estimations of $i_{s\alpha}$, $i_{s\beta}$, $\varphi_{r\alpha}$, $\varphi_{r\beta}$, R_r and L_m by measuring $i_{s\alpha}$, $i_{s\beta}$ and ω_m from points of view the estimation

© The Institution of Engineering and Technology 2020

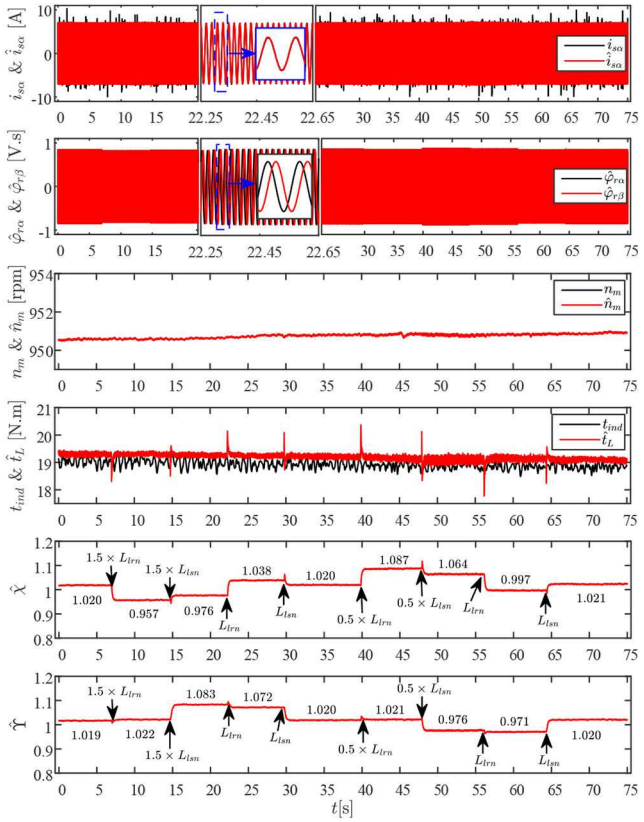


Fig. 12 *Real-time experimental results of proposed EKF for changes in Leakage Inductances*

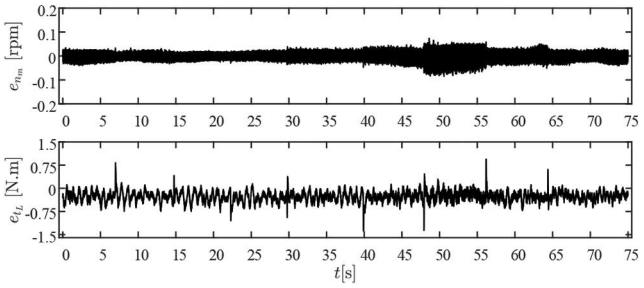


Fig. 13 *Real-time experimental results of EKF based estimation error associated with n_m and t_L for changes in leakage inductances*

performance and execution time. For the estimation performance, they are operated under the same operating conditions including step-like changes in t_L at constant speed and using the same value of the elements in $\boldsymbol{Q}$ and $\boldsymbol{R}$ for the corresponding the state as below:

$\boldsymbol{Q}^{\text{8th order(proposed)EKF}} = \text{diag}\{10^{-10}, 10^{-10}, 10^{-12}, 10^{-12}, 10^{-5}, 10^{-4}, 10^{-5}, 10^{-5}\}$, $\boldsymbol{R}^{\text{8th order(proposed)EKF}} = \text{diag}\{10^{-4}, 10^{-4}, 10^{-4}\}$, $\boldsymbol{Q}^{\text{6th orderEKF}} = \text{diag}\{10^{-10}, 10^{-10}, 10^{-12}, 10^{-12}, 10^{-5}, 10^{-5}\}$, and $\boldsymbol{R}^{\text{6th orderEKF}} = \text{diag}\{10^{-4}, 10^{-4}\}$.

The resulting performances are presented in Figs. 14 and 15, and it is observed that $\hat{i}_{s\alpha}$, $\hat{\chi}$, $\hat{\Upsilon}$, and $|\hat{\varphi}_r| = \sqrt{(\hat{\varphi}_{r\alpha}^2 + \hat{\varphi}_{r\beta}^2)}$ in the eighth order (proposed) EKF converge more quickly to their measured or expected value with less relative errors ($e_{|\hat{\varphi}_r|}^{\text{relative}}$, $e_{\hat{\chi}}^{\text{relative}}$ and $e_{\hat{\Upsilon}}^{\text{relative}}$) after the instant change occurs, considering ones in the sixth order EKF. The obtained results confirm the effectiveness of the proposed EKF, which utilises the extended measurement vector (z) and thus providing additional estimations of ω_m and t_L over the sixth order EKF. On the other hand, both EKFs are realised by using MATLAB Simulink C/C++ S-Function block, and the execution times of the eighth order (proposed) and the sixth order EKF are measured as 25.32 and 16.03 μs, respectively. Namely, the eighth order (proposed) EKF provides the additional and improved

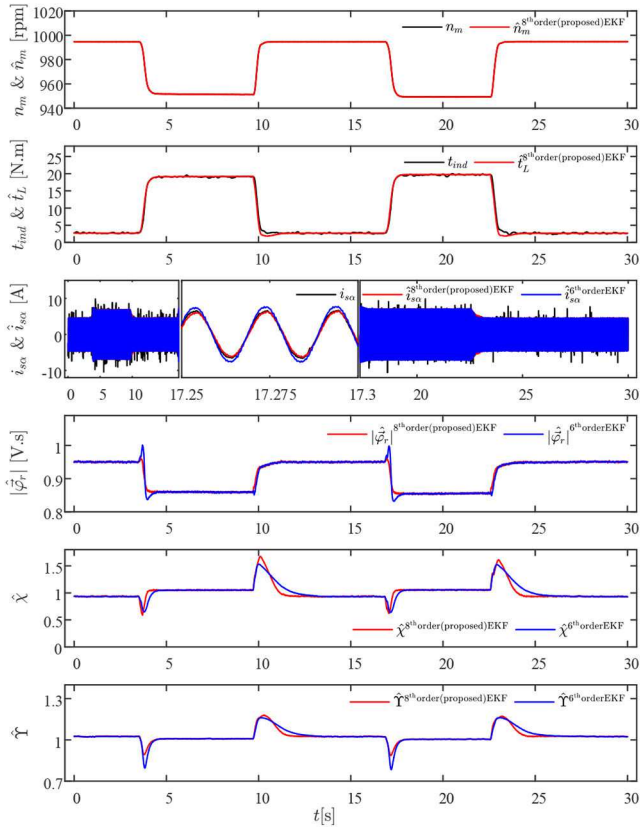


Fig. 14 *Real-time experimental results for comparison of the eighth order (proposed) and the sixth order EKFs*

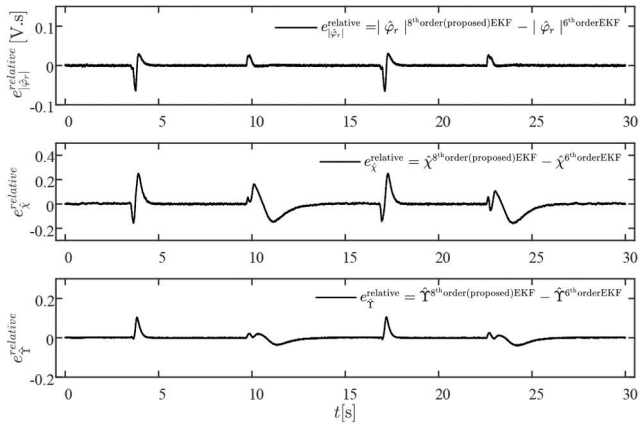


Fig. 15 *Real-time experimental results of relative errors ($e_{|\hat{\varphi}_r|}^{relative}$, $e_{\hat{\chi}}^{relative}$, and $e_{\hat{\Upsilon}}^{relative}$) for comparison of the eighth order (proposed) and the sixth order EKFs*

estimations with the increased but feasible execution time, which is usual in the literature for the solution of the model based state(s) and parameter(s) estimation problems for IMs. Furthermore, the eighth order (proposed) EKF perform gives the estimated uncertainties ($\hat{\Upsilon}$) related to L_m in addition to the states estimated by the seventh order EKF-based past study in [26], by extending the measurement vector (z).

7 Conclusion

In this study, a novel EKF algorithm with the help of a single eighth order IM model including the extended measured states for the on-line estimations of $i_{s\alpha}$, $i_{s\beta}$, $\varphi_{r\alpha}$, $\varphi_{r\beta}$, ω_m, t_L, R_r and L_m is introduced

© The Institution of Engineering and Technology 2020

- To solve the performance deteriorations due to the variations in t_L as in the past EKF based speed-sensored studies such as [16–18].
- Not to utilise switching technique between two seventh order IM models as in the BI-EKF technique ([22, 23]) which makes the tuning elements of noise covariance matrices difficult and challenging and increases the computational burden, the required memory, and the design complexity in terms of a standard EKF algorithm utilising a single IM model for obtaining the increased number of estimated states and parameters.

For these aims, ω_m is assigned as a state by using the equation of motion in the IM model; thus, together with estimating t_L, the rotor speed error and the stator current errors are taken into account in calculating or correcting the estimations of the unmeasured states in the proposed EKF algorithm in this paper. The results obtained from both computer simulations and real-time experiments confirm the superiority of the proposed EKF algorithm over the past EKF-based studies whose performances are deteriorated by the changes in t_L as in [16–18]. The real-time experimental results also verify that the eighth order (proposed) EKF algorithm presents the additional and improved estimations with the increased but feasible execution time according to the sixth order EKF implemented in this paper.

8 References

[1] Comanescu, M.: 'Single and double compound manifold sliding mode observers for flux and speed estimation of the induction motor drive', *IET Electr. Power Appl.*, 2014, **8**, (1), pp. 29–38

[2] Bogosyan, S., Barut, M., Gokasan, M.: 'Braided extended Kalman filters for sensorless estimation in induction motors at high-low/zero speed', *IET Control Theory Appl.*, 2007, **1**, (4), pp. 987–998

[3] Bolognani, S., Peretti, L., Zigliotto, M.: 'Parameter sensitivity analysis of an improved open-loop speed estimate forinduction motor drives', *IEEE Trans. Power Electron.*, 2008, **23**, (4), pp. 2127–2135

[4] Cao, P., Zhang, X., Yang, S.*, et al.*: 'Reactive-power-based MRAS for online rotor time constant estimation in induction motor drives', *IEEE Trans. Power Electron.*, 2018, **33**, (12), pp. 10835–10845

[5] Jouili, M., Jarray, K., Koubaa, Y.*, et al.*: 'Luenberger state observer for speed sensorless ISFOC induction motor drives', *Electr. Power Syst. Res.*, 2012, **89**, pp. 139–147

[6] Wang, H., Liu, Y.C., Ge, X.: 'Sliding-mode observer-based speed-sensorless vector control of linear induction motor with a parallel secondary resistance online identification', *IET Electr. Power Appl.*, 2018, **12**, (8), pp. 1215–1224

[7] Alsofyani, I.M., Idris, N.R.N.: 'Lookup-table-based DTC of induction machines with improved flux regulation and extended Kalman filter state estimator at low-speed operation', *IEEE Trans. Ind. Inf.*, 2016, **12**, (4), pp. 1412–1425

[8] Jafarzadeh, S., Lascu, C., Fadali, M.S.: 'State estimation of induction motor drives using the unscented Kalman filter', *IEEE Trans. Ind. Electron.*, 2012, **59**, (11), pp. 4207–4216

[9] Popovic, V., Oros, D., Vasic, V.*, et al.*: 'Tuning the rotor time constant parameter of IM using the minimum order recursive linear least square estimator', *IET Electr. Power Appl.*, 2019, **13**, (2), pp. 266–276

[10] Shinohara, K., Nagano, T., Arima, H.*, et al.*: 'Online tuning method of stator and rotor resistances in both motoring and regenerating operations for vector-controlled induction machines', *Electr. Eng. Jpn.*, 2001, **135**, (1), pp. 56–64

[11] Karanayil, B., Rahman, M.F., Grantham, C.: 'Stator and rotor resistance observers for induction motor drive using fuzzy logic and artificial neural networks', *IEEE Trans. Energy Convers.*, 2005, **20**, (4), pp. 771–780

[12] Salmasi, F.R., Najafabadi, T.A.: 'An adaptive observer with online rotor and stator resistance estimation for induction motors with one phase current sensor', *IEEE Trans. Energy Convers.*, 2011, **26**, (3), pp. 959–966

[13] Mapelli, F.L., Tarsitano, D., Cheli, F.: 'MRAS rotor resistance estimators for EV vector controlled induction motor traction drive: analysis and experimental results', *Electr. Power Syst. Res.*, 2017, **146**, pp. 298–307

[14] Yang, S., Ding, D., Li, X.*, et al.*: 'A novel online parameter estimation method for indirect field oriented induction motor drives', *IEEE Trans. Energy Convers.*, 2017, **32**, (4), pp. 1562–1573

[15] Yang, S., Ding, D., Li, X.*, et al.*: 'A decoupling estimation scheme for rotor resistance and mutual inductance in indirect vector controlled induction motor drives', *IEEE Trans. Energy Convers.*, 2019, **34**, (2), pp. 1033–1042

[16] Talla, J., Peroutka, Z., Blahnik, V.*, et al.*: 'Rotor and stator resistance estimation of induction motor based on augmented EKF'. 2015 Int. Conf. on Applied Electronics (AE), Pilsen, Czech Republic, 2015, pp. 253–258

[17] Demir, R., Barut, M., Yildiz, R.*, et al.*: 'EKF based rotor and stator resistance estimations for direct torque control of induction motors'. 2017 Int. Conf. on Optimization of Electrical and Electronic Equipment (OPTIM) 2017 Intl Aegean Conf. on Electrical Machines and Power Electronics (ACEMP), Brasov, Romania, 2017, pp. 376–381

[18] Demir, R., Barut, M., Yıldız, R.: 'Reduced order extended kalman filter based parameter estimations for speed-sensored induction motor drive', *Pamukkale Univ. J. Eng. Sci.*, 2018, **24**, (8), pp. 1464–1471

[19] Yildiz, R., Barut, M., Zerdali, E.: 'A comprehensive comparison of extended and unscented Kalman filters for speed-sensorless control applications of induction motors', *IEEE Trans. Ind. Inf.*, 2020, **10**, (16), pp. 6423–6432

[20] Yin, Z., Li, G., Zhang, Y.*, et al.*: 'A speed and flux observer of induction motor based on extended Kalman filter and Markov chain', *IEEE Trans. Power Electron.*, 2017, **32**, (9), pp. 7096–7117

[21] Barut, M., Bogosyan, S., Gokasan, M.: 'Experimental evaluation of braided EKF for sensorless control of induction motors', *IEEE Trans. Ind. Electron.*, 2008, **55**, (2), pp. 620–632

[22] Barut, M., Demir, R., Zerdali, E.*, et al.*: 'Real-time implementation of bi input-extended kalman filter-based estimator for speed-sensorless control of induction motors', *IEEE Trans. Ind. Electron.*, 2012, **59**, (11), pp. 4197–4206

[23] Inan, R., Barut, M.: 'Bi input-extended Kalman filter-based speed-sensorless control of an induction machine capable of working in the field-weakening region', *Turkish J. Electr. Eng. Comput. Sci.*, 2014, **22**, (3), pp. 588–604

[24] Choi, D.H., Shin, M.H., Lee, T.K.*, et al.*: 'Vector control of an induction motor for the field weakening region with tuning of the magnetizing inductance'. Proc. of Power Conversion Conf. – PCC '97, Nagaoka, Japan, 1997, vol. 1, pp. 107–112

[25] Zaky, M.S., Khater, M.M., Shokralla, S.S.*, et al.*: 'Wide-speed-range estimation with online parameter identification schemes of sensorless induction motor drives', *IEEE Trans. Ind. Electron.*, 2009, **56**, (5), pp. 1699–1707

[26] Barut, M., Bogosyan, S., Gokasan, M.: 'An EKF-based estimator for the speed sensorless vector control of induction motors', *Electr. Power Compon. Syst.*, 2005, **33**, (7), pp. 727–744

[27] Proca, A.B., Keyhani, A.: 'Identification of variable frequency induction motor models from operating data', *IEEE Trans. Energy Convers.*, 2002, **17**, (1), pp. 24–31

[28] 'IEEE standard test procedure for polyphase induction motors and generators', IEEE Std 112-1996, 1997, pp. 1–64.IEEE Std 112-1996

[29] Rajput, S., Bender, E., Averbukh, M.: 'Simplified algorithm for assessment equivalent circuit parameters of induction motors', *IET Electr. Power Appl.*, 2020, **14**, (3), pp. 426–432

[30] Cacciato, M., Consoli, A., Scarcella, G.*, et al.*: 'Estimation of the leakage and magnetizing inductances of induction motors'. 2009 13th European Conf. on Power Electronics and Applications, Barcelona, Spain, 2009, pp. 1–10

[31] Silvino, J.L., Rabelo, B.C.: 'An improved estimation of the induction machine leakage inductances', *IEEE Trans. Ind. Electron.*, 1999, **46**, (5), pp. 1040–1042

[32] Ranta, M., Hinkkanen, M., Luomi, J.: 'Inductance identification of an induction machine taking load-dependent saturation into account'. 2008 18th Int. Conf. on Electrical Machines, Vilamoura, Portugal, 2008, pp. 1–6

© The Institution of Engineering and Technology 2020